THE AGE DIFFERENCE BETWEEN THE GLOBULAR CLUSTER SUBPOPULATIONS IN NGC 4472

Thomas H. Puzia

Sternwarte der Universität Bonn, Auf dem Hügel 71, D-53121 Bonn, Germany; and UCO/Lick Observatory, University of California at Santa Cruz, Santa Cruz, CA 95064; tpuzia@astro.uni-bonn.de

Markus Kissler-Patig[1]

European Southern Observatory, Karl-Schwarzschild-Strasse 2, D-85748 Garching bei München, Germany; and UCO/Lick Observatory, University of California at Santa Cruz, Santa Cruz, CA 95064; mkissler@eso.org

Jean P. Brodie[2]

UCO/Lick Observatory, University of California at Santa Cruz, Santa Cruz, CA 95064; brodie@ucolick.org

AND

John P. Huchra[2]

Harvard-Smithsonian Center for Astrophysics, 60 Garden Street, MS 20, Cambridge, MA 02138-1516; huchra@cfa.harvard.edu

ABSTRACT

The age difference between the two main globular cluster subpopulations in the Virgo giant elliptical galaxy NGC 4472 (M49) has been determined using *Hubble Space Telescope* WFPC2 images in the F555W and F814W filters. Accurate photometry has been obtained for several hundred globular clusters in each of the two main subpopulations, down to more than 1 mag below the turnover of their luminosity functions. This allows precise determinations of both the mean colors and the turnover magnitudes of the two main subpopulations. By comparing the data with various population synthesis models, the age-metallicity pairs that fit both the observed colors and magnitudes have been identified. The metal-poor and the metal-rich globular clusters are found to be coeval within the errors (~ 3 Gyr). If one accepts the validity of our assumptions, these errors are dominated by model uncertainties. A systematic error of up to 4 Gyr could affect this result if the blue and the red clusters have significantly different mass distributions. However, that one subpopulation is half as old as the other is excluded at the 99% confidence level. The different globular cluster populations are assumed to trace the galaxy's major star formation episodes. Consequently, the vast majority of globular clusters (and by implication the majority of stars) in NGC 4472 formed at high redshifts but by two distinct mechanisms or in two episodes. The distance to NGC 4472 is determined to be 15.8 ± 0.8 Mpc, which is in excellent agreement with six of the seven Cepheid distances to Virgo Cluster spiral galaxies. This implies that the spiral and elliptical galaxies in the main body of Virgo are at the same distance.

Key words: galaxies: formation — galaxies: individual (NGC 4472) — galaxies: star clusters — globular clusters: general

1. INTRODUCTION

1.1. *Star Formation in Early-Type Galaxies Traced by Globular Cluster Formation*

Arguably the two most important open questions about the formation of early-type galaxies are when they formed their first stars and when they assembled dynamically. While the latter question is probably best answered by observations at intermediate and high redshift, the answer to the former is likely to be found from observations in the more local universe.

A number of studies have estimated the epoch of star formation by comparing observations of the diffuse stellar component in nearby and low-redshift galaxies with stellar population models (e.g., Renzini 1999 and Bender 1997 for reviews). However, the use of diffuse star light has two main disadvantages. First, it is very difficult to disentangle different stellar populations, and, second, a relatively recent but (in mass) unimportant star formation episode can dominate the luminosity-weighted quantities used to derive the star formation history.

Both these problems are bypassed when globular clusters are used to study the main epochs of star formation. In nearby galaxies, individual globular clusters appear as point sources, and can be characterized by a single age and a single metallicity. Distinct populations can easily be identified (e.g., in a color distribution of the globular cluster system) and the mean properties of the subpopulations can be determined. The relative numbers in each subpopulation will also indicate the relative importance of each star formation episode.

There is strong support for the assumption that globular cluster formation traces star formation. First, major star formation observed today in interacting galaxies is accompanied by the formation of massive young star clusters (e.g., Schweizer 1997, although their exact nature is still under debate; see Brodie et al. 1998). Second, the specific frequency (i.e., number of globular clusters normalized to the galaxy star light; see Harris & van den Bergh 1981) is constant to within a factor of 2 in almost all galaxies (see compilation in Ashman & Zepf 1998), which points to a link between star and cluster formation. Moreover, although this relation seems to fail in giant ellipticals, McLaughlin (1999) has shown that the number of globular clusters is in fact proportional to the total mass, and the number per unit mass is extremely constant from galaxy to galaxy. Finally,

---

in less violent star formation episodes, Larsen & Richtler (1999) have shown that the number of young star clusters in spirals is directly proportional to the current star formation rate.

To first order, globular clusters are likely to be excellent tracers for the star formation episodes in early-type galaxies.

1.2. Several Epochs of Star Formation

There is now evidence for multiple globular cluster subpopulations in a number of luminous, early-type galaxies (Zepf & Ashman 1993; Ashman & Zepf 1998 for a recent compilation). The origin of these subpopulations is still under debate (e.g., Gebhardt & Kissler-Patig 1999) but it seems clear that the main subpopulations formed in different star formation episodes, perhaps at different epochs. In the best studied galaxies with multiple populations, the number of clusters in each subpopulation is roughly equal, suggesting that these galaxies have had more than one *major* star formation episode. The overall evidence from photometry and more recently from spectroscopy (Kissler-Patig et al. 1998a; Cohen, Blakeslee, & Ryzhov 1998) suggests that in the cluster giant ellipticals the main subpopulations are old. In other noninteracting early-type galaxies, the nondetection of subpopulations, either due to their absence or to a conspiracy of age and metallicity, leads to the same conclusion: no major globular cluster (i.e., star) formation has occurred since $z \simeq 1$ (Kissler-Patig, Forbes, & Minniti 1998b).

There have been a few previous attempts to determine the relative age difference between globular cluster subpopulations. In the S0 galaxy NGC 1380, Kissler-Patig et al. (1997) derived an age difference of around 3 to 4 Gyr between the halo and bulge globular clusters. In M87, Kundu et al. (1999) estimated the metal-rich clusters to be 3 to 6 Gyr younger than the metal-poor ones. As a comparison, in the Milky Way, the difference between halo and bulge/disk globular clusters seems to be small (less than 1 Gyr: Ortolani et al. 1995; around 17%: Rosenberg et al. 1999).

Deriving relative ages from photometry alone is complicated by the fact that broadband colors suffer from an age-metallicity degeneracy (e.g., Worthey 1994). One possible solution to this problem is to measure several quantities that are affected differently by age and metallicity and to combine the results. For example, most broadband colors are more affected by metallicity than by age. On the other hand, optical magnitudes for a given mass are more affected by age than they are by metallicity. A combination of both can break the age-metallicity degeneracy when the mass distributions are known (see § 4.1).

Both a mean color as well as a "mean magnitude" can be measured for a globular cluster subpopulation. The mean color is simply the mean color of the globular cluster subsample and can be determined from a color distribution of the globular clusters. The turnover (TO) point of the globular cluster luminosity function (GCLF) of a given subpopulation can be used as its "mean magnitude." The absolute TO magnitude of the GCLF has been found to be fairly constant from one globular cluster system to the next in a wide variety of galaxy types and environments with a peak at $M_V^{TO} \simeq -7.5$ (see Whitmore 1997 and Ferrarese et al. 2000 for summaries). Three quantities affect the TO value: age, metallicity, and mass. The effects of age and

metallicity on the magnitude of a single stellar population were quantified by Ashman, Conti, & Zepf (1995) using population synthesis models from Bruzual & Charlot (1995). The mean mass influences the TO magnitude because the TO of the GCLF corresponds to a break in the globular cluster mass distribution (e.g., McLaughlin & Pudritz 1996). That is, if the characteristic mass (at which the slope of the power-law mass function changes) varies, the TO magnitude will be affected. However, the mass distributions seem to be extremely similar from galaxy to galaxy and are expected to be very similar for different subpopulations within the same galaxy, if destruction processes are the dominant mechanism for shaping the mass distribution and had time enough to act on both subpopulations. We will come back to this point in § 4.2.

Neither the mean color nor the TO magnitude alone can be used to derive the age and metallicity of a globular cluster population because of the above-mentioned degeneracy. This paper marks the first time that both the mean color *and* the TO magnitude of each globular cluster subpopulation have been simultaneously compared to single stellar population (SSP) models (see § 4.1) in order to distinguish age and metallicity. Deep high-quality photometry is required to reliably determine the mean color and the TO magnitude (implying good photometry below this TO point), and clean globular cluster samples are needed, i.e., good discrimination between globular clusters and foreground/background contamination is essential. The Wide Field and Planetary Camera 2 (WFPC2) on board the Hubble Space Telescope (*HST*) provides the most accurate photometric data available and makes such an analysis feasible.

1.3. Globular Clusters in NGC 4472

For this first study we selected a galaxy that hosts a populous globular cluster system, which provides good number statistics even after the sample is split into the different subpopulations.

NGC 4472 (M49), the brightest giant elliptical galaxy in the Virgo Cluster, is located in the center of a subgroup within the cluster and is of Hubble type E2. It is one of the brightest early-type galaxy within 20 Mpc, with an absolute magnitude of $M_V \simeq -22.6$ (see Table 1 for other characteristics). It hosts 6300 ± 1900 globular clusters (Geisler, Lee, & Kim 1996). The specific frequency of globular clusters is $S_N = 5.6 \pm 1.7$, close to the average for bright cluster ellipticals.

TABLE 1

GENERAL PROPERTIES OF NGC 4472

Parameter	Value
RA (2000.0)[a]	$12^h29^m46^s.79 \pm 1^s.25$
Decl. (2000.0)[a]	$+08°00'01".50 \pm 1".25$
m_V [b]	8.41 ± 0.06 mag
$V-I$ [c]	1.24 ± 0.01 mag
$B-V$ [b]	0.96 ± 0.01 mag
M Type[b]	E2/S0(2)
V_{helio} [b]	868 ± 8 km s^{-1}
Distance[d]	15.8 ± 0.8 Mpc

[a] Laurent-Muehleisen et al. (1997).
[b] RC3v9 (de Vaucouleurs et al. 1991).
[c] Poulain (1988).
[d] This paper.

Previous photometric studies of the globular cluster system of this galaxy include those of Cohen (1988, Gunn-Thuan photometry), Couture, Harris, & Allwright (1991, Johnson photometry), Ajhar, Blakeslee, & Tonry (1994, Johnson photometry), Geisler et al. (1996, Washington photometry), and Lee, Kim, & Geisler (1998, Washington photometry).

The two most recent studies were the first to obtain a comprehensive enough data set to allow the identification and characterization of the two main globular cluster sub-populations. The mean metallicities of the two sub-populations were found to be [Fe/H] $\simeq -1.3$ and -0.1 dex for the blue and red peak, respectively. The observed metallicity gradient (Δ[Fe/H]/$\Delta \log r \simeq -0.4$ dex [log (arcsec)]$^{-1}$) in the system is mostly due to the radially varying ratio of these two populations. The metal-rich component is spatially more concentrated and has the same ellipticity as the galaxy star light, while the metal-poor component is more extended and spherical. These two components can be loosely associated with the "halo" and "bulge" of NGC 4472, suggesting different formation mechanisms for these galaxy structures and the associated clusters. The relative ages of these two components is the subject of this paper.

The paper is structured as follows. In § 2 we present the observation and data reduction. Section 3 contains details of the data analysis; color, and turnover magnitude determinations, etc. Section 4 compares the results to stellar evolutionary models to determine the age difference between the subpopulations. In § 5 we derive a new distance to NGC 4472 using the TO magnitude method. Section 6 summarizes the results.

2. OBSERVATIONS AND DATA REDUCTION

2.1. Observations

The WFPC2 images of NGC 4472 were obtained from two data sets. The nuclear pointing was taken from West-phal et al. (*HST* program GO.5236) and was complemented by our own pointings to the north and south of the galaxy (*HST* program GO.5920, PI: Brodie) which were offset in declination by $2'16''$ and $2'49''$ from the center of the galaxy, respectively. The data are summarized in Table 2.

2.2. Data Reduction
2.2.1. Image Processing

We used calibrated science images returned by the Space Telescope Science Institute.[3] The basic reduction was carried out in IRAF.[4] The images were combined with the task CRREJ of the STSDAS package. The Brodie data set consists of paired, dithered exposures and was thus registered by shifting the second of each image pair by $0''506$ (i.e., five pixels for the WF chips, 12 pixels for the PC chips) with the task IMSHIFT.

Using the standard aperture radius of Holtzman et al. (1995) of $0''5$, we tested for any magnitude error that might

be introduced by incomplete shifting of frames. This error was found to be less than 0.0003 mag for both filters and is therefore negligible.

2.2.2. Photometry

The photometry was carried out using the source extraction software SExtractor (version 2.0.19) by Bertin & Arnouts (1996). For the purpose of object selection only, the images were convolved with the instrumental point-spread function (PSF) to improve the detection efficiency. The PSF for each filter was taken from the *HST* Handbook (version 4.0), using the PSFs (pixel-centered) at 600 nm for F555W and at 800 nm for F814W. The selection criteria were set to two connected pixels, 2 σ above the background computed in a 32 × 32 pixel^2 grid. Magnitudes were measured in two pixels and $0''5$ radius apertures (see also next section). Objects in common on the V and I frames were identified and matched. The positions on the sky of all objects were computed using the task METRIC in the STSDAS package.

The calibration and transformation to the Johnson-Cousins V and I filters followed Holtzman et al. (1995) and corrections for charge transfer efficiency and gain (7 e^- per analog-to-digital converter unit [ADU] for all our data) were applied. In what follows, the magnitude errors will *not* include the less than 4% systematic error potentially introduced by the calibration. The values measured in the $0''5$ radius apertures were used to compute the final magnitudes in order to avoid having to apply an additional correction to the data.

2.2.3. Extended Objects Calibration

Globular clusters at the distance of the Virgo galaxy cluster are expected to be resolved. Milky Way globular clusters have typical half-light radii between 3 and 10 pc (e.g., Harris 1996[5]), corresponding to $0''04$ to $0''13$ at 16 Mpc distance. Indeed, most of our globular cluster candidates have FWHM measurements (as returned by SExtractor) slightly larger than measured for unresolved objects. This in turn implies that the photometric corrections proposed by Holtzman et al. (1995) for unresolved objects will not be valid for converting from the $0''5$ radius aperture to the total globular cluster magnitude.

New rough corrections were derived as follows. We computed 30 × 30 pixel^2 normally sampled PSFs in V and I for a WF chip using the TinyTim (version 4.4) program by Krist & Hook (1997)[6], and we convolved these PSFs with Hubble laws of different core radii ($0''05$, $0''1$, $0''2$, $0''6$). Note that these PSFs include the convolution with the diffusion kernel (see Krist & Hook 1997), which is not well defined. This kernel introduces an intrinsic smoothing to the optical PSF (as seen at the top of the CCD chip) because of charge diffusion.

The cumulative light distributions of these modeled objects were compared with those of a set of isolated globular cluster candidates of various luminosities and chip positions taken from our data. The data in I match almost perfectly the PSF convolved with a Hubble law of $0''1$ core (corresponding to ~8 pc at a distance of 16 Mpc), while the V data lie in between the PSF models convolved with $0''05$ and $0''1$ Hubble laws.

TABLE 2

SUMMARY OF OBSERVATIONS

Prg. ID + PI	R.A.	Decl.	F555W Exp. Time[a] (s)	F814W Exp. Time[a] (s)
GO.5236 Westphal	12 29 48.73	+07 59 55.85	1800	1800
GO.5920 Brodie (north)......	12 29 45.22	+08 02 34.38	2200	2300
GO.5920 Brodie (south)......	12 29 45.20	+07 57 30.11	2200	2300

NOTE.—Units of right ascension are hours, minutes, and seconds, and units of declination are degrees, arcminutes, and arcseconds.

[a] Effective exposure time, after images were stacked.

The same procedure, using 10 times oversampled PSFs without applying any diffusion kernel, yielded best fitting Hubble-core radii of 0″.3 for I data and 0″.1 for the V data. Until the behavior of the diffusion kernel is better understood (wavelength dependencies, etc.), it is possible that a systematic core-radius error of about 0″.1 (~ 8 pc) may be present in all radius estimation studies of Virgo globular clusters using WFPC2 data. Nonetheless, we used the normally sampled and diffusion-kernel convolved PSFs for our analysis.

The modeled light profiles (see Fig. 1), unlike the real data, provide high enough signal-to-noise to determine the extrapolation from an 0″.5 radius to the total V and I magnitudes. The derived corrections are applied to the 0″.5 radius aperture measurements in addition to the Holtzman point source correction of $C = 0.1$. These additional corrections are $C_V = 0.050 \pm 0.015$ and $C_I = 0.080 \pm 0.010$ (which results in a color correction of $C_{(V-I)} = 0.030 \pm 0.018$). The errors reflect the uncertainty in matching the data with the models and the accuracy of the extrapolation

to infinity of our fit to the light profile. The errors do not include, for example, the fact that the core and the half-light radii of different globular clusters may vary significantly. In general, our data were calibrated applying the correction for point sources of $C = 0.10$. When additional corrections were included, they are specifically mentioned in the text. Note that the corrections are systematic, i.e., they do not affect *relative* magnitudes. Therefore, the accuracy with which we are able to determine age-metallicity *differences* should not be seriously affected.

2.2.4. Artificial Star/Cluster Experiments

Artificial star/cluster experiments were carried out using the tasks STARLIST and MKOBJECTS from the IRAF package ARTDATA. We added 1000 objects per run in both the V and I images, and we computed 400 runs, resulting in 400,000 artificial objects per filter and covering the whole parameter space of background values. Both objects modeled by a WF chip PSF and objects modeled by the same PSF but convolved with Hubble laws of core radius 0″.05 (V) and 0″.1 (I) were added. All objects had a color of $V - I = 1.1$, previous tests with 5000 objects having shown no significant variations among the completeness curves for $V - I = 0.9$, 1.1, and 1.3.

The selection completeness was computed for objects found on both the V and I images. All detected objects that passed our selection criteria (see § 2.2.5) and all input objects were sorted by their background value and subdivided in 10 background-value bins for V and I, respectively. A *skewed Fermi function*

$$F(x) = \frac{ax + b}{1 + \exp{(x - c)^d}} \qquad (1)$$

was fitted to all completeness histograms for each background bin. A smoothing procedure using a low-pass filter gives nearly the same results. The 50% completeness limits lie around $V \simeq 25.5$ and $I \simeq 24.5$ for the lowest background value. The 50% completeness magnitude falls off continuously with a growing background (see Fig. 2).

The artificial-object experiments also allowed us to determine the error in the photometry and to test the accuracy with which the FWHM of objects can be recovered as a function of magnitude. Typical FWHM values were deduced for extended objects that are a good match to the FWHM values of our globular cluster candidates.

FIG. 1.—Curves of growth for PSF models and selected data. The curves represent different models. *Solid line* = raw TinyTim PSF; *long-dashed line* = Hubble law (0″.05 core radius) ⊗ PSF; *short-dashed line* = Hubble law (0″.1 core radius) ⊗ PSF; *dot-dashed line* = Hubble law (0″.2 core radius) ⊗ PSF; *open circles* = the selected globular cluster data (13 candidates in V and 15 in I).

2.2.5. Globular Cluster Selection Criteria

Object selection criteria were applied to our extracted data to provide a clean sample of globular cluster candi-
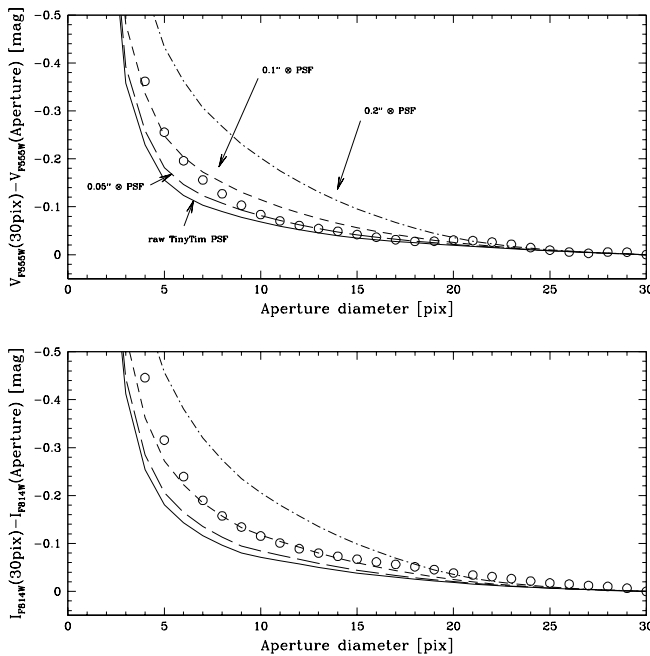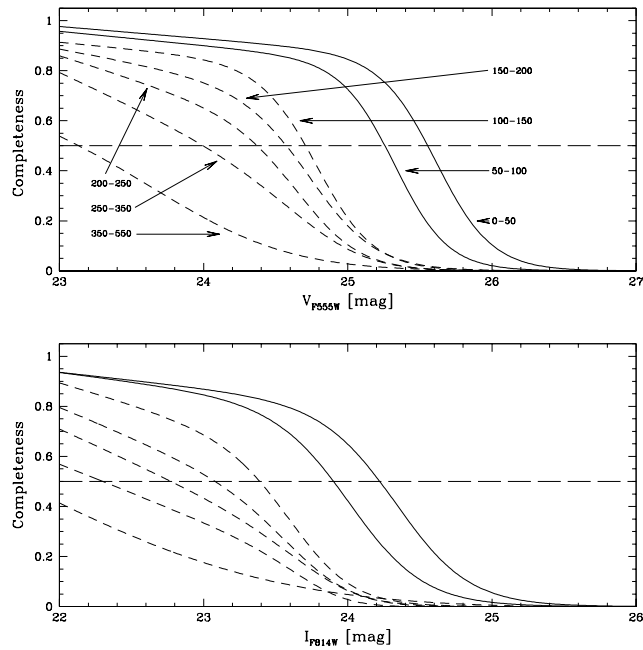
FIG. 2.—Completeness curves for the central pointing (*dashed lines*) and for the north and south pointings (*solid lines*). The central images have much higher background values than the northern and southern pointings. Each curve refers to a particular background value bin, i.e., from faint to bright magnitudes in counts: 0–50, 50–100, 150–200, 200–250, 250–350, 350–550.

FIG. 3.—Background contamination histograms for the V_{F606W} and I_{F814W} band resulting from the HDF-N. The unshaded histograms show the background object luminosity distribution as obtained from HDF-N directly, while the shaded ones show the same data after applying our criteria. The lines are exponential least-square fits to the small histograms. In order to ensure a reasonable fit, we set the upper limit for the magnitude range at the 50% completeness level quantified during the completeness tests. Using the exponential law, the integrated number of background objects is ~30 up to the 50% completeness limit in both filters.

dates for further analysis. Only objects that met the color cut of $0.5 < V{-}I < 1.8$ and a magnitude cut of $V \leq 25.5$ and $I \leq 25.2$ were included, so that some of the red unresolved galaxy nuclei were rejected (see Fig. 3). In addition, a FWHM cut in the range 0.75 pixels < FWHM < 2.5 pixels was applied. We also calculated the magnitude difference obtained through apertures of 0.5 and 3 pixel radii, which allowed us to distinguish between point-source objects and extended objects such as globular clusters (e.g., Schweizer et al. 1996). A very rough upper cut of $\Delta(0.5 - 3) > 1.0$ was used.

The neural network of SExtractor (version 2.0.19), i.e., the CLASS parameter, was used to supplement the above selection criteria. This parameter was defined for well-sampled images (Bertin & Arnouts 1996). Since the WFPC2 provides undersampled images, the reliability of the CLASS parameter is reduced. We applied only the selection criterion CLASS < 1.0 to our data. A test showed that for objects brighter than the 50% completeness level the CLASS parameter cut reliably eliminates point sources and cosmic rays.

Our final list of globular cluster candidates includes 705 objects in V and I. This is 38% of the initially extracted sample. An electronic list of the globular-cluster candidates is available from the authors.

2.2.6. Background Contamination

One significant advantage of HST data over ground-based observations is high spatial resolution, which allows high-confidence rejection of extended objects. However, background contamination is still expected. In order to determine the background fraction in our data, we ran the same extraction and selection criteria for the Hubble Deep
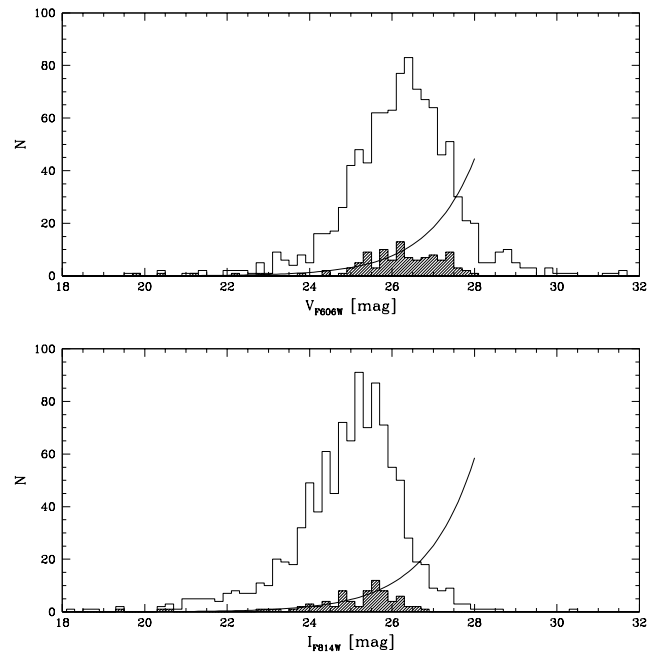
Field-North (HDF-N; Williams et al. 1996) images. Since the HDF-N has galactic coordinates of $l = 125.89$ and $b = +54.83$ while our exposures have $l = 286.92$ and $b = +70.20$, we might overestimate the contamination due to foreground stars using this approach, although foreground star contamination is, in any case, expected to be negligible. We obtained from the HST Archive images in the F606W and F814W filters with exposure times of 15,200 s and 20,200 s, respectively. These images are far deeper than our own. Both magnitudes for F606W and F814W were transformed to Johnson V and Cousins I magnitudes. We determined contamination histograms with and without the application of our selection criteria in order to establish their reliability. Exponential laws have been fitted to the histograms after applying the rejection criteria, up to the 50% completeness limits. The exponential laws act as input for our "improved maximum-likelihood" code (see § 3.2.1).

Note the efficiency of our selection criteria. Nearly all background objects are removed from the data up to the 50% completeness magnitude. The contamination is less than 5% for both the V_{F606W} and I_{F814W} filters (see Fig. 3).

We stress again that all the above corrections were applied to the full sample, i.e., differential values between subsamples remain unaffected even if small systematic effects have been introduced.

3. ANALYSIS

Our goal is to determine the mean colors and turnover magnitudes of the luminosity functions of the two main globular cluster subpopulations in both the V and the I

filters. These colors and magnitudes can then be compared to the predictions of population synthesis models for given ages and metallicities.

3.1. Mean Colors

In order to determine the mean colors of the sub-populations we selected from the total sample objects with small photometric errors. The application of a magnitude cut at $V = 23.75$ resulted in errors $\Delta(V-I) < 0.05$. We further applied an upper magnitude cut at $V = 20.0$ (corresponding to $M_V \simeq -11.2$ at the distance of Virgo), in order to exclude any foreground star contamination, and a broad cut in color $[0.8 < (V-I) < 1.8]$ to isolate the region where globular clusters are expected. The color-magnitude diagram of our sample is shown in Figure 4, together with the box (*dotted lines*) of preselected objects (see § 2.2.5). A $(V-I)$ histogram of those selected objects is shown in Figure 5.

Formally, a key underlying assumption is that the color (metallicity) does not significantly vary with magnitude (mass) within a subpopulation. This appears to be the case as far as can be tested with our data.

A KMM test (Ashman, Bird, & Zepf 1994) was run on our constrained subsample. The test determines the confidence with which bimodality can be said to be present, the most likely relative contribution of each population to the sample, and the peaks (i.e., mean colors) of each subpopulation. We find that the color distribution is bimodal at the greater than 99.99% confidence level. The relative contributions of objects to the selected sample (see § 2.2.5) are 282 and 423 in the blue and red populations respectively. The peaks of the color distribution lie at $(V-I) = 0.99 \pm 0.01$ and 1.24 ± 0.01 for the blue and red subpopulations, respectively. Formally, the peaks can be determined with an accuracy of 0.005 mag. The error adopted here reflects the range of values derived by varying the selection criteria (i.e., magnitude and color cuts).
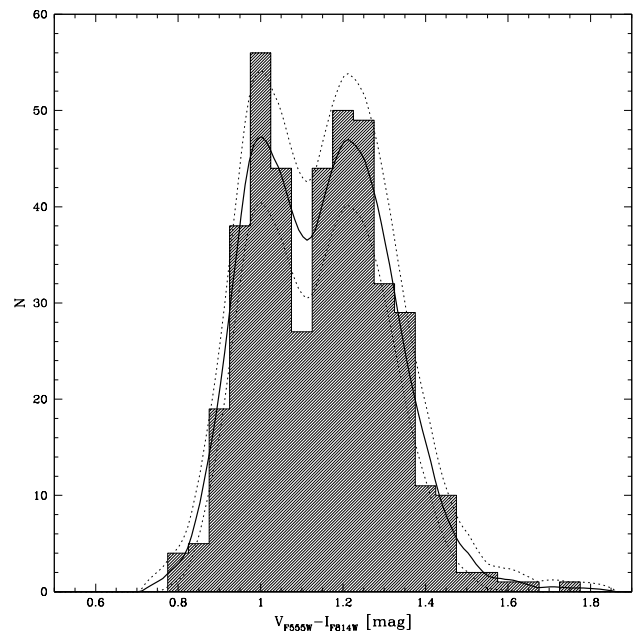
FIG. 5.—Color distribution of globular clusters in NGC 4472. A bimodal distribution is found to be present at the 99.99% confidence level using the KMM mixture-modeling algorithm (Ashman et al. 1994). The two peaks lie at 0.99 ± 0.01 and 1.24 ± 0.01 (0.93 ± 0.01 and 1.18 ± 0.01 corrected for reddening and aperture). A further analysis using a density estimation technique (kernel estimator with an Epanechnikov kernel) yields color peaks at $V-I = 1.00 \pm 0.01$ and 1.22 ± 0.01. The solid line depicts the derived distribution function with statistical upper and lower error limits (*short-dashed lines*).

Two fitting modes were used: (1) forcing identical dispersions (homoscedastic fit) and (2) allowing independent dispersions (heteroscedastic fit). We note that substantially better fits (in terms of reduced χ^2) are obtained if the dispersions of the blue and red distributions are allowed to differ and that the red population seems to have a color distribution twice as broad as the blue one ($\sigma_{blue} \simeq 0.06$, $\sigma_{red} \simeq 0.12$).

We estimated the peak colors with yet another method that avoids the assumption of a Gaussian distribution for each color peak (intrinsic to the KMM code). We computed the density distribution in color of the objects with the help of a kernel estimator using the Epanechnikov kernel (e.g., Gebhardt & Kissler-Patig 1999). We used $h_{opt} = 0.043$ for the smoothing parameter (see Silverman 1986 for detailed discussion), an average of the optimal smoothing parameters for the blue and red peak [h_{opt}(blue) = 0.023 and h_{opt}(red) = 0.063] estimated from the σ-guess of KMM for both modes. The density distribution is overplotted in Figure 5. A biweight fit to each peak returns $(V-I) = 1.00 \pm 0.01$ and 1.22 ± 0.01, in perfect agreement with the results from the KMM code.

To obtain the mean colors of the peaks, the above $(V-I)$ values need to be corrected for the calibration offset described in § 2.2.3 [$\Delta(V-I) = 0.030 \pm 0.018$] and for a Galactic reddening toward NGC 4472 of $E(B-V) = 0.0224$ (Schlegel, Finkbeiner, & Davis 1998), i.e., $E(V-I) = 1.3E(B-V) = 0.029$ (following Dean, Warren, & Cousins 1978). Note that the *relative* color difference, later used to derive the age difference, is only affected by these corrections in second order. The final, corrected mean
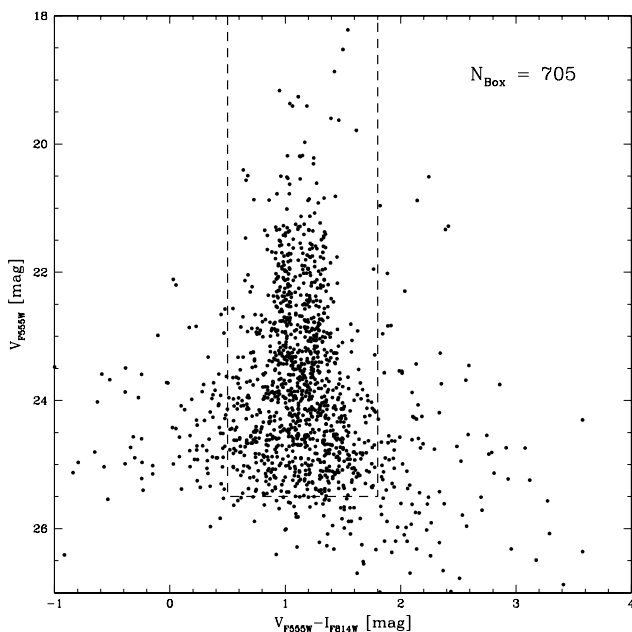

FIG. 4.—Color-magnitude diagram of globular clusters in NGC 4472. The box delineates the initial cuts made to the raw data prior analysis. Enclosed are 705 globular cluster candidates.

colors of the two populations are $(V-I)_0 = 0.93 \pm 0.02$ and $(V-I)_0 = 1.18 \pm 0.02$.

3.2. Turnover Magnitudes

The TO magnitudes of the luminosity functions for the blue and red subpopulation were individually determined in each filter using a maximum-likelihood approach (see Secker 1992). The changing background counts over our whole sample motivated us to develop a version of Secker's "maximum-likelihood estimator," which includes background variations. We calculated the completeness as a function of magnitude and background noise as described in § 2.2.4. This improved code, described below, was used to derive the peak of the magnitude distribution for each filter and each subpopulation.

Secker (1992) showed that the GCLF of the Milky Way and M31 was best represented analytically with the Student's t_5-function

$$t_5(m \,|\, m_0, \sigma_t) = \frac{8}{3\sqrt{5}\pi\sigma_t} \left[1 + \frac{(m - m_0)^2}{5\sigma_t^2} \right]^{-3} . \quad (2)$$

We adopted the Student's t_5 function as the most appropriate distribution for the GCLF of NGC 4472 since it matches the tails of the distribution better than a Gaussian function. The difference in the result using the one or the other function, however, is very small.

3.2.1. Improved Maximum Likelihood

Usually, a data set of n independent observations, such as a sample of magnitudes $M = (m_1, m_2, \ldots, m_n)$, is distributed in an unknown way. Assuming a distribution function $\phi(M \,|\, \Omega)$ that describes the distribution of data properly and depends on q parameters $\Omega = (p_1, p_2, \ldots, p_q)$ (particularly the turnover magnitude m_0 and the dispersion σ_t) the likelihood function $l(\Omega \,|\, M) = \phi(M \,|\, \Omega)$ is considered as a function l of Ω for a given data set M. The likelihood function is

$$l(\Omega \,|\, M) = \prod_{i=1}^{n} \phi(m_i \,|\, \Omega) . \quad (3)$$

For convenience, during the calculation the logarithmic likelihood function is used. During the evaluation the best set of parameters $\bar{\Omega}$ is found if

$$\left. \frac{\partial l(\Omega)}{\partial \Omega} \right|_{\Omega = \bar{\Omega}} = 0 . \quad (4)$$

For a detailed treatment of maximum-likelihood theory see, for instance, Bevington & Robinson (1992).

Our improved maximum-likelihood code, based on Secker's (1992) code, takes into account the influence of the background-noise level ρ on the completeness function $I(m, \rho)$, in addition to the magnitude. Similarly, the photometric error function $\varepsilon(m, \rho)$ now also depends on these two variables. The distribution function is

$$\phi(m \,|\, m_0, \sigma_t, \rho) = K\Phi(m \,|\, m_0, \sigma_t, \rho) + (1 - K)B(m \,|\, \rho), \quad (5)$$

where m_0 is the turnover magnitude of the given distribution and σ_t is its dispersion (note: $\sigma_{\mathrm{Gauss}} = 1.291\sigma_{t_5}$), while ρ is the background noise for the evaluation position on the chip. $K = N_{\mathrm{GC}}/(N_{\mathrm{GC}} + N_{\mathrm{HDF}})$ is the mixing parameter, i.e., the fraction of globular-cluster candidates in the whole data set including the background objects. Note that in our case K is close to 1.

It is necessary to normalize all the functions used, which is implicitly accomplished by

$$\Phi(m \,|\, m_0, \sigma_t, \rho) = I(m \,|\, \rho)\left(\int t_5(m' \,|\, m_0, \sigma_t)\varepsilon(m \,|\, m', \sigma_t)dm' \right) \quad (6)$$

and

$$B(m \,|\, \rho) = I(m \,|\, \rho)b(m) , \quad (7)$$

where $b(m)$ is the background contamination function obtained from the HDF data. ε is the photometric error function

$$\varepsilon(m \,|\, m', \rho) = \frac{1}{\sqrt{2\pi}\sigma(m', \rho)} \exp\left[\frac{(m - m')^2}{2\sigma(m', \rho)^2} \right], \quad (8)$$

which is assumed to introduce Gaussian errors to the distribution function ϕ with a magnitude and background noise dependent dispersion

$$\sigma(m, \rho) = \sqrt{10^{0.4(m-a)} + \rho^2 10^{0.8(m-b)}} . \quad (9)$$

The parameters a and b can be estimated with sufficient accuracy from a two-dimensional fit to the photometric errors obtained from the artificial star experiments. They act as input parameters to our code.

The need to account for the variable background, i.e., the need for the improved code, is best seen in Figure 2. The selection completeness as a function of magnitude is plotted for a few typical values of background counts found in our data sets. The 50% completeness limits shift to brighter magnitudes with increasing background, i.e., photon noise.

Alternatively, one could approximate a "mean" completeness by distributing the artificial stars with the same density profile as the globular clusters, without including the background as a parameter in the maximum-likelihood analysis. The approach we have adopted is the more accurate solution to the problem. The package described above is available as an IRAF task from the authors.

3.2.2. Maximum-Likelihood Estimations

The maximum-likelihood routine of Drenkhahn (1999) was used to determine the TO magnitudes. Our completeness functions fitted down to the 50% completeness levels ($V_{\mathrm{faintest}} \simeq 25.5$, $I_{\mathrm{faintest}} \simeq 24.5$) were used as the input. The data were convolved with the errors as a function of magnitude (see eq. [6]). The input globular cluster data were selected as described in § 2.2.5. From KMM mixture modeling we determined that $(V-I) = 1.1$ is the best value for separating blue and red clusters. For the analysis we split the full data set into the central (Westphal) pointing and the combination of the halo (Brodie) pointings, since these two data sets had slightly different exposure times, i.e., slightly different limiting magnitudes/completenesses. The TO magnitudes for the individual pointings are given in Table 3, together with an average for the whole sample. The globular cluster luminosity functions are shown in Figure 6. The values in Table 3 still need to be corrected for Galactic extinction ($A_V = 0.069$ and $A_I = 0.040$) and the additional aperture correction (see § 2.2.3), however, these corrections do not affect the relative difference between the TO magnitudes.

We varied the input completeness and noise limits to the maximum-likelihood code; the resulting TO magnitudes all lie within less than 0.15 mag.

TABLE 3

TURNOVER MAGNITUDES AND DISPERSIONS FOR EACH SUBPOPULATION
LUMINOSITY FUNCTION

Filter	Population	M_{TO}[a]	ΔM_{TO}[a]	σ_{t_5}	$\Delta\sigma_{t_5}$	N_{GC}
Total sample:						
V...	Blue	23.62	0.09			
	Red	24.13	0.11			
I...	Blue	22.48	0.07			
	Red	22.90	0.11			
Westphal (inner) sample:						
V...	Blue	23.55	0.15	1.21	0.10	118
	Red	23.97	0.19	1.42	0.10	180
I...	Blue	22.62	0.21	1.24	0.14	129
	Red	22.83	0.19	1.39	0.10	174
Brodie (outer) sample:						
V...	Blue	23.68	0.11	1.36	0.09	175
	Red	24.30	0.13	1.39	0.09	232
I...	Blue	22.33	0.08	1.14	0.07	178
	Red	22.97	0.13	1.39	0.08	213

[a] TO magnitudes are corrected neither for reddening nor for the aperture correction discussed in § 2.2.3. The corrections for galactic reddening are $A_V = 0.069$ and $A_I = 0.040$. The corrections for aperture, in addition to the correction of Holtzman $C = 0.1$ (which is already included) are $C_V = 0.050 \pm 0.015$ and $C_I = 0.080 \pm 0.010$ (which are not included here).

As a consistency check, we attempted to reproduce the mean (uncorrected) colors of the subpopulations ($V-I = 0.99 \pm 0.01$ and 1.24 ± 0.01) by computing the differences between the V and I TO magnitudes for a given population. We obtained $(V-I)_{TO} = 1.14 \pm 0.11$ for the blue population and $(V-I)_{TO} = 1.23 \pm 0.16$ for the red population, where the errors are the errors of the V and I TOs taken in quadrature. The color for the blue population derived in this way is somewhat redder than that derived from the color distribution but the values agree to within the errors for both populations.

3.2.3. Monte Carlo Simulations

The error in the TO magnitude directly affects the error in the estimation of the age difference between the two subpopulations (see § 4.1). We carried out Monte Carlo simulations to check whether our relatively modest sample sizes (which were as low as 118 to 232 objects when divided into inner and outer samples) affect the results significantly and to establish the associated error.

The blue and red samples were simulated in the V filter using the number of objects in each sample and assuming a Gaussian distribution with the parameters derived above. These artificial samples were input into the maximum-likelihood code. The 68% confidence levels (1 σ) on the TO magnitudes, from 10^4 iterations, were 0.10 and 0.13 for the blue and red samples, respectively. These are in good agreement with the 1 σ errors returned by the maximum-likelihood estimation.

3.3. Comparison with Previous Observations

The derived colors and TO magnitudes were compared to previous results from other groups.

3.3.1. Mean Colors

Geisler et al. (1996) derived metallicity peaks for the blue and red subpopulations from Washington photometry. They found peaks at $[Fe/H] = -1.3 \pm 0.38$ dex and -0.1 ± 0.38 dex for the blue and red subsamples, respectively. Our colors, derived in § 3.1, can also be translated into metallicities. However, large errors are introduced by the particular choice of a conversion relation of the $(V-I)$ color into metallicity. Using the relation given by Kissler-Patig et al. (1998a) $[Fe/H] = [-(4.50 \pm 0.30) + (3.27 \pm 0.32)(V-I)]$, which is tuned to reflect the nonlinear behavior at high metallicity, we obtain metallicities of $[Fe/H] = -1.45 \pm 0.43$ dex and -0.64 ± 0.49 dex. These values are somewhat lower than, but within the errors of, the values derived by Geisler et al. (1996). Using the transformation of Kundu & Whitmore (1998), $[Fe/H] = -5.89 + 4.72(V-I)$, our data yield metallicities of $[Fe/H] = -1.50 \pm 0.05$ dex and $[Fe/H] = -0.32 \pm 0.05$ dex. The error corresponds to our photometric error in $(V-I)$ only. No calibration error of Kundu & Whitmore is considered. The metallicity calibration of Couture et al. (1990), $[Fe/H] = -6.096 + 5.05(V-I)$, gives the somewhat larger values of $[Fe/H] = -1.39 \pm 0.05$ dex and -0.11 ± 0.05 dex, similar to those derived by Geisler et al. (1996).

3.3.2. TO Magnitudes

TO magnitudes have been derived by several groups, but only for the whole sample (i.e., an average of the red and blue populations) and in different filters. Previous results should be compared to the average of our blue and red sample, with the necessary correction for reddening and aperture size: $V_0 = 23.76 \pm 0.20$ (including the error on the TO magnitude and the error on the aperture correction). Furthermore, all other groups assumed $E(B-V) = 0.00$ toward NGC 4472 (using Burstein & Heiles (1982, 1984), while we adopted the Schlegel et al. (1998) map from DIRBE/IRAS whose zero point is offset by 0.020 in $E(B-V)$. Our value would translate into $V_0 = 23.83 \pm 0.20$ if we assumed $E(B-V) = 0.00$.

Using the Washington-Johnson transformation of Geisler (1996), $V \simeq T_1 + 0.5$, Lee et al.'s (1998) result translates into $V_0 = 23.81 \pm 0.07$, in excellent agreement with our result. We note that Lee et al. investigated their blue and red samples separately but did not find any significant difference in their TO magnitudes to within $\simeq 0.15$ mag. However, their analysis was less rigorous in this respect than ours, and their data suffered from more background contamination, as is expected for ground-based observations.

Harris et al. (1991) derived $B_{TO} = 24.78 \pm 0.22$ with a three-parameter Gaussian fit to the GCLF. Using $B-V \simeq 0.8$ for the total population of globular clusters, this translates into $V_{TO} = 23.98 \pm 0.22$. Ajhar et al. (1994) derived $R_{TO} = 23.3 \pm 0.2$ (read off their Fig. 14), which, for $V-R \simeq 0.5$, translates into $V_{TO} = 23.8 \pm 0.2$. These results are in very good agreement with our determination.

3.4. Radial Dependencies
3.4.1. TO Magnitudes as a Function of Radius

Variation in the TO magnitude with radius within a population can occur if the mean age, metallicity, or mass changes with radius. Large age and metallicity gradients are ruled out by the absence of any significant color gradient in the subpopulations (see Fig. 7). A systematic change in the mean mass with radius could be caused by destruction processes shaping the globular cluster mass function. These are more important toward the center of the galaxy (e.g., recent work by Vesperini 1998 and Gnedin & Ostriker 1997), and significant changes are only expected within $\simeq 5$ kpc
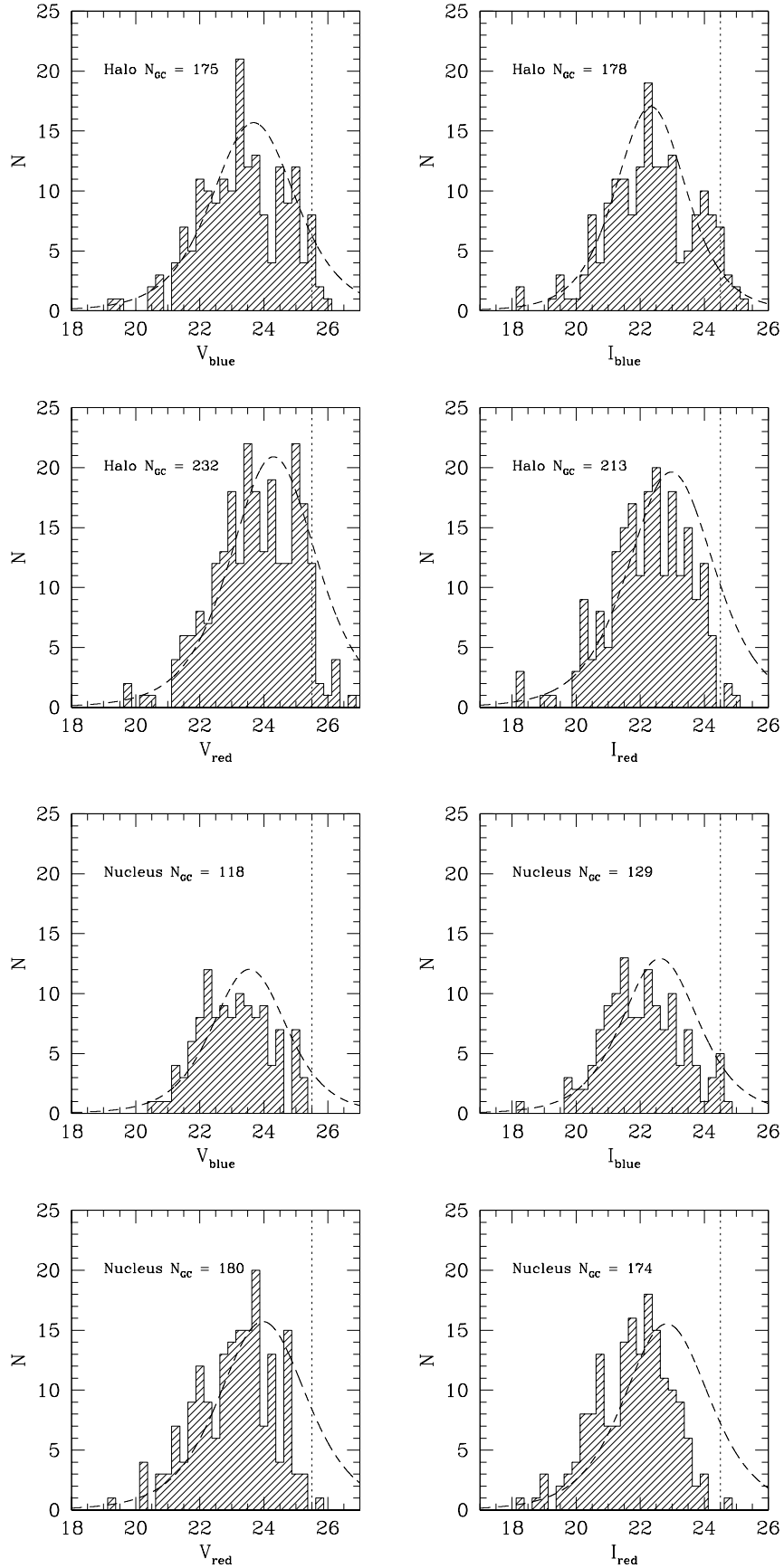
FIG. 6.—Globular cluster luminosity functions of the halo (Brodie) pointings (*top four plots*) and central (Westphal) pointing (*bottom four plots*). The number of clusters that went into the histograms up to the faintest completeness limit are indicated. The histograms are shown for the selected globular clusters, uncorrected for completeness and background variations (see text). The dashed curves are the best fitting t_5 functions as derived from our maximum-likelihood analysis, taking into account completeness and background corrections. The t_5 functions were arbitrarily normalized. The vertical dotted lines mark our 50% completeness limit at the lowest background value.
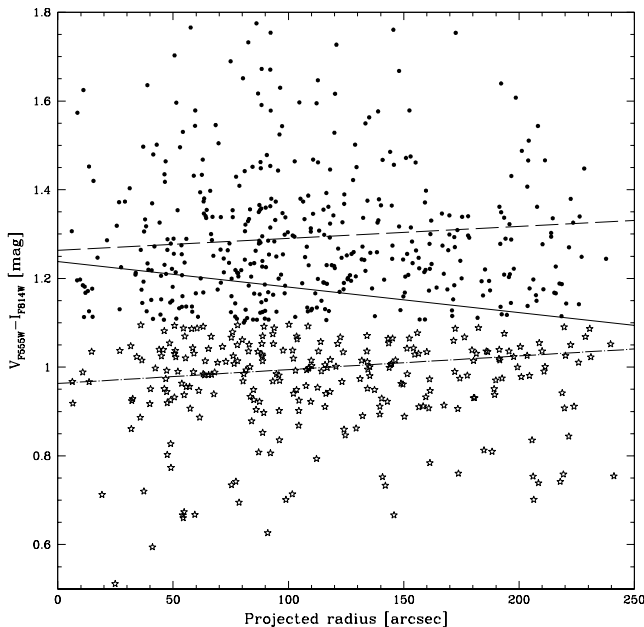
FIG. 7.—Radial distributions of the red (*open circles*) and blue (*stars*) globular clusters. The dashed line represents the best weighted linear least-square fit to the red population. The dot-dashed line gives the best fit to the blue population. The solid line shows the best fit for the entire globular cluster population. The gradient is twice as large as for each subpopulation.

of the center ($\simeq 65''$ at 16 Mpc). There the peak of the GCLF is expected to be brighter by up to $\simeq 0.3$ magnitudes, and the peak should be sharper as a consequence of the preferential destruction of low-mass clusters. Our inner sample (Westphal data) includes clusters at projected radii between $2''$ and $127''$ with a mean of $65''$ and our outer sample (Brodie data) includes clusters at projected radii between $76''$ and $252''$ with a mean of $160''$. Differences are therefore expected between these two samples. For the blue population, the TO magnitude varies from the inner to the outer regions by 0.12 ± 0.20 and -0.29 ± 0.25 in V and I respectively. The weighted mean is -0.04 ± 0.16, i.e., we observed no brightening of the TO toward the center, although the uncertainty is on the order of the expected variation. For the red population the TO magnitude varies from the inner to the outer region by 0.33 ± 0.17 and 0.14 ± 0.25 in V and I, respectively. Formally, the TO appears brighter by 0.27 ± 0.14 (weighted mean) for the inner red population. We do not see any changes in the dispersion of the GCLF to within the errors.

This result is probably not yet secure enough to be worth commenting on in depth. However, a difference between the red and blue population could occur, for example, if the blue and red clusters are on different orbits. Sharples et al. (1998) found tentative evidence for the blue clusters in NGC 4472 having a higher velocity dispersion and higher rotation than the red ones. Kissler-Patig & Gebhardt (1998) found a similar (but firmer) result for M87, another giant elliptical that hosts enough globular clusters for such an analysis. If indeed the blue clusters are preferentially on tangential orbits, while the red clusters are preferentially on radial orbits, destruction processes would be more efficient for the red population.

Finally, we note that Harris et al. (1998) and Kundu et al. (1999) also looked for this effect in M87. Kundu at el. even

looked for trends in the blue and red populations separately. Neither group found any brightening of the GCLF toward the center of M87, but note again that the uncertainties in the measurements are still of the order of the expected signal.

3.4.2. Color as a Function of Radius

We looked for color gradients within the subpopulations using a weighted least squares fitting routine. In addition to the color cuts ($0.5 < V-I < 1.1$ and $1.1 < V-I < 1.8$), the samples were cut at $V = 24.8$ to provide at least 50% completeness even in the central regions. The results are plotted in Figure 7, together with a fit for the total sample. The derived gradients are $\Delta(V-I)/\Delta \log r = 0.015 \pm 0.004$ mag [log (arcsec)]$^{-1}$ and 0.013 ± 0.007 mag [log (arcsec)]$^{-1}$ for the blue and red population respectively. Different color and magnitude cuts scatter these results within 0.01 mag [log (arcsec)]$^{-1}$. Any positive gradients in the subpopulations are either very small or nonexistent. For the whole sample, however, we find a clear negative gradient of $\Delta(V-I)/\Delta \log r = -0.029 \pm 0.07$ mag [log (arcsec)]$^{-1}$, corresponding to a metallicity gradient of $\Delta[\text{Fe/H}]/\Delta \log r \simeq -0.15 \pm 0.02$ dex [log (arcsec)]$^{-1}$ (somewhat dependent on the color-metallicity relation used).

We confirm Geisler et al.'s (1996) result, that this gradient is caused by the changing ratio of red to blue clusters as a function of radius, rather than an overall decrease in metallicity with radius. Quantitatively, we find a somewhat smaller gradient than reported by Geisler et al. (1996), who found $\Delta[\text{Fe/H}]/\Delta \log r \simeq -0.4$ dex [log (arcsec)]$^{-1}$. This is probably due to our smaller radial coverage and our use of a less metallicity-sensitive color. Indeed, our sample extends to only $250''$ while Geisler et al.'s data extend out to $\simeq 500''$. The ratio of blue to red clusters varies by only $\simeq 10\%$ from our inner to outer regions, as derived from a comparison of their cumulative radial distributions.

A similar situation is seen in M87, for which Harris et al. (1998) report no color gradient within $60''$, and Kundu et al. (1999) report a weak gradient of $\Delta(V-I)/\Delta \log r = -0.017 \pm 0.012$ mag [log (arcsec)]$^{-1}$ within $100''$. However, Lee & Geisler (1993) report a strong gradient ($\Delta[\text{Fe/H}]/\Delta \log r = -0.65 \pm 0.17$ dex [log (arcsec)]$^{-1}$) over $500''$ radius.

3.5. Globular Cluster Sizes

The high resolution of *HST* allows us to study the *relative* sizes (see § 2.2.3) of the globular cluster candidates using the parameter $\Delta(0.5 - 3)$ (see § 2.2.5). For extended objects the magnitude difference in two different apertures will appear large as the light profile contributes a nonnegligible amount of light to the outer aperture. The opposite is the case if the light profile is narrow. For this analysis, we restricted ourselves to clusters found on the Wide Field (WF) camera chips to avoid the problematic conversion between the WF and the Planetary Camera (PC). Figure 8 presents the histogram of globular cluster sizes for both the blue and red subpopulations. The median values for these two distributions point to a systematic size difference between the blue and the red globular clusters. The median values for the blue and red populations are $m_\Delta = 2.06 \pm 0.01$ mag and $m_\Delta = 2.02 \pm 0.01$ mag, respectively, indicating that the blue globular clusters are substantially larger than the red globular clusters. A maximum-
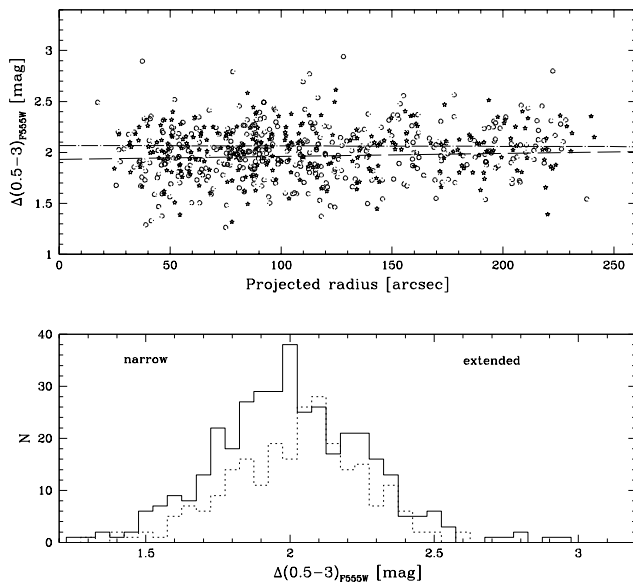
FIG. 8.—*Top panel*: Radial globular cluster size distribution for blue (*open stars*) and red (*open circles*) globular clusters. The dot-dashed line is the best least-square fit to the blue subpopulation while the dashed line gives the best fit to the red subpopulation. *Bottom panel*: Histogram of relative globular cluster sizes for the red population (*solid histogram*) and the blue population (*dashed histogram*). The sizes of the blue globular clusters are substantially larger than those of the red.

likelihood estimation of the mean and its error yields the same results.

Interestingly, in both NGC 3115 (Kundu & Whitmore 1998) and M87 (Kundu et al. 1999), the blue clusters also appear significantly larger than the red ones. The authors suggest this is due to different radial distributions for the red and blue clusters, noting that Galactic globular clusters with larger galactocentric distances have larger half-light radii (van den Bergh 1994).

To study the radial dependence of globular cluster size, we plotted the size parameter $[\Delta(0.5 - 3)]$ versus radius and found no gradients: $\Delta(0.5 - 3) = 2.07(\pm 0.03) - 0.5$ $(\pm 3.2)10^{-4}r$ where r is the radius in arcseconds, and $\Delta(0.5 - 3) = 1.93(\pm 0.03) - 2.9(\pm 2.7)1$, for the blue and red clusters, respectively (see also Fig. 8). The difference between blue and red clusters is present at all radii. We therefore speculate that the different sizes are a relic of the different formation processes, unless the red and blue clusters are on significantly different orbits. For example, the red clusters could be preferentially on radial orbits and be systematically more affected than the blue clusters by the central potential during their close passage near the galaxy center.

4. AGE DIFFERENCE BETWEEN THE MAIN SUBPOPULATIONS

4.1. *Comparison with the Models*

We compare our results (TO magnitude and mean color) with various population synthesis models in order to derive the age *difference* between the blue and red globular cluster subpopulations.

We used the new models from Maraston (1998) as well as the most recent models from the Göttingen group (Kurth, Fritze-v. Alvensleben, & Fricke 1999) and the models from Bruzual & Charlot (1996) and Worthey (1994). In each case we compared our data with every available initial mass

function (IMF), i.e., usually the Salpeter IMF and a multi-slope IMF. The full range of metallicities was used as well as the necessary age range. Since we are only interested in age *differences*, the exact normalization of the absolute magnitude, which is dependent on mass and mass-to-light ratio (M/L) ratio for a given IMF, is not important. The grids in Figures 9 through 12 can, therefore, be somewhat arbitrarily shifted in the y-direction. In the following, we fixed the grids in the y-direction such that the oldest subpopulation lies on the oldest computed isochrone (15 Gyr or 16 Gyr). Further, we arbitrarily set the blue population to $V = 0$ and $I = 0$ in order to compare the different models directly. There is no freedom in the x-direction since the color is not mass dependent and the grid is fixed in $V - I$ for a given stellar population.

For the mean colors of the blue and red subpopulations we used the colors derived in § 3.1. The TO values used were the ones derived for the full sample (see Table 3). We stress again that additive corrections to both the blue and red TO magnitudes (i.e., reddening correction, potential systematic errors, aperture corrections) only influence the difference as second order effects, if at all, and are not a concern.

However, we make two important underlying assumptions. We assume that the M/L ratios for blue and red clusters are only dependent on age and metallicity (i.e., the IMFs of the blue and red clusters are similar). Second, we assume that blue and red cluster populations have the same underlying mass distribution (by which we mean globular cluster masses, not IMFs). Under these assumptions, TO magnitudes are influenced only by age and metallicity. We briefly discuss the validity of these assumptions and the errors they potentially introduce.

4.1.1. *M/L and Mass Distribution Assumptions*

Kissler-Patig et al. (1998b) review the empirical reasons for expecting the mass distributions and M/L's to be similar among various subpopulations. Briefly, the M/L assumption is essentially that both blue and red clusters have similar IMFs, at least below 1 $M_\odot$ where it influences our result. Observations so far for globular clusters in the Local Group seem to confirm this picture (e.g., Dubath & Grillmair 1997). In the case of the mass distribution, globular cluster formation seems to follow a universal mechanism (e.g., Elmegreen & Efremov 1997). The constancy of the TO magnitude from galaxy to galaxy (e.g., the review by Whitmore 1997) and the observed mass distributions of young clusters (e.g., brief review by Schweizer 1997) support this picture.

The possibility that size differences might indicate different formation processes for blue and red clusters was discussed in § 3.5. It is not clear, however, whether it is only the mean sizes or also the mean masses that are affected. Moreover, our assumption would fail if, despite similar mass distributions at formation, blue and red clusters are affected differently by destruction processes. There is a hint (see § 3.4) that this might be the case in the inner region, where the difference between the blue and the red TO magnitudes is smaller by 0.32 ± 0.24 (combining the V and I information) than in the outer region. (We note for completeness that an age gradient in the population would have the same observable effect as a mass gradient). If this effect is real, the TO difference of the total sample, as used, could be affected by a 0.1 to 0.2 mag systematic error. We estimate that this empirical determination gives about the right order of mag-

nitude for the potential systematic error in our method and, in what follows, we will assume a potential systematic error of $\simeq 0.2$ mag, which translates into roughly 4 Gyr.

Note that for similar M/L values of the blue and red clusters, such a difference of 0.2 mag would translate into only a 20% difference in the mass characterizing the TO. Irrespective of the accuracy needed for our study, blue and red clusters *have* roughly similar mass distributions.

4.1.2. Avoiding Assumptions about the Masses

For completeness, we mention a method for checking the validity of these assumptions and a method for avoiding them.

For the chosen filters, age and characteristic mass influence the TO far more than metallicity, which is fairly well determined by the color. Therefore, one could determine the mean mass difference (and check the above assumption) by obtaining an independent estimate of the mean age difference. An independent age estimate could be obtained with spectroscopy of a large number of globular clusters and the measurement of an age-sensitive absorption-line index. Several tens of Hβ measurements in each subpopulation would allow the mean Hβ value to be determined to within less than 0.1 Å, which would translate into an accuracy in the mean age difference of $\simeq 2$ Gyr. This in turn would allow us to verify that the characteristic TO masses of the red and blue populations lie within 10% to 20% of each other.

An alternative method for determining the mean age difference without making any assumptions about the mass distributions would be to use mass-independent quantities

that depend only on age and metallicity. Broadband colors are such quantities. A plot similar to Figures 9 through 12, but in a color-color plane, would remove any uncertainties due to different mass distributions. However, it is impossible to find two colors in the optical and NIR spectrum that disentangle age and metallicity as efficiently as the color/TO magnitude combination.

4.1.3. Comparison with Maraston (1998)

In Figure 9, we compare our results to the models of Maraston (1998). She computed single-burst–population models with a Salpeter (1955) and multislope IMF (Gould et al. 1998) for metallicities $Z = 0.001, 0.006, 0.02$, and 0.04, and ages up to 15 Gyr. We refer the reader to the original paper for further details of the modeling.

The derived age difference, which is quoted in the following as $(\text{age}_{\text{blue}}) - (\text{age}_{\text{red}})$, varies between approximately -0.3 Gyr (Gould et al. IMF, I band) and approximately $+2.4$ Gyr (Gould et al. IMF, V band), with errors of about 2.7 Gyr (1 σ). Within the errors, the blue and red population appear coeval, with a formal difference of $+0.7 \pm 1.8$ Gyr (straight mean of the four computed differences with their dispersion shown as the error). A 3 σ limit on the age difference would be around 6 Gyr.

4.1.4. Comparison with Kurth et al. (1999)

In Figure 10, we compare our results with the recent models of Kurth et al. (1999). They computed single-burst models with a Salpeter (1955) and a Miller & Scalo (1979) IMF for six metallicities between $Z = 0.0001$ and 0.05 and ages up to 16 Gyr.
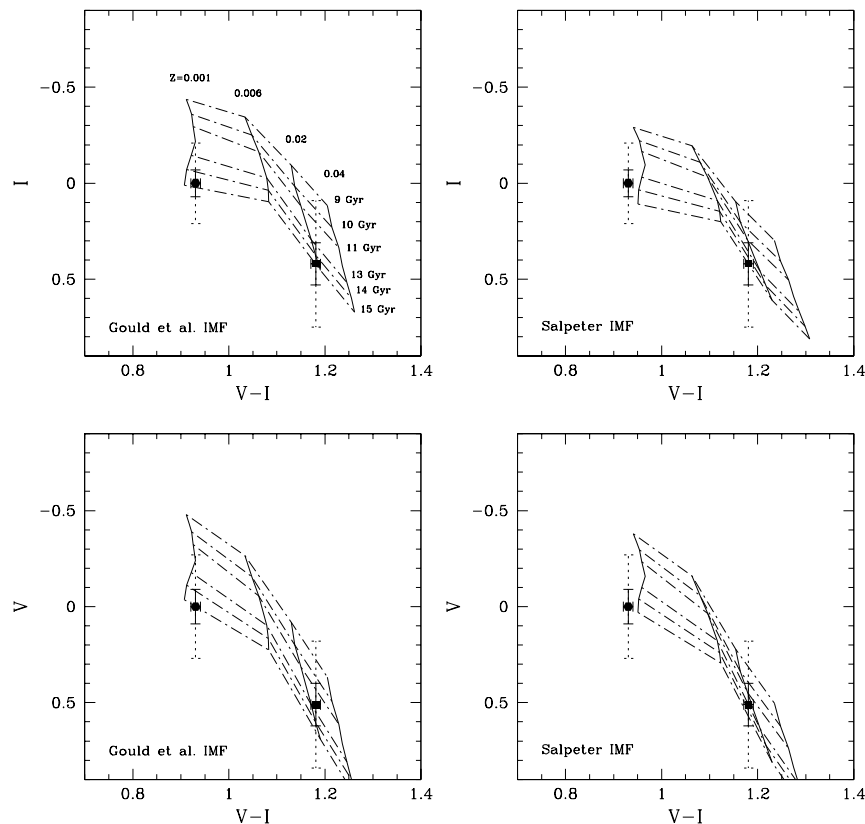

FIG. 9.—Maraston's (1998) simple stellar population models. *Top panels*: I-band data. *Bottom panels*: V-band data. The solid grid lines represent isometallicity tracks of $Z = 0.001, 0.006, 0.02, 0.04$. Dash-dotted lines are isochrones of 9, 10, 11, 13, 14, and 15 Gyr. Solid error bars represent 1 σ errors and dashed error bars refer to 3 σ errors. The averaged maximum age difference ($\text{age}_{\text{blue}} - \text{age}_{\text{red}}$) is $\Delta T = 0.7 \pm 1.8$ Gyr.
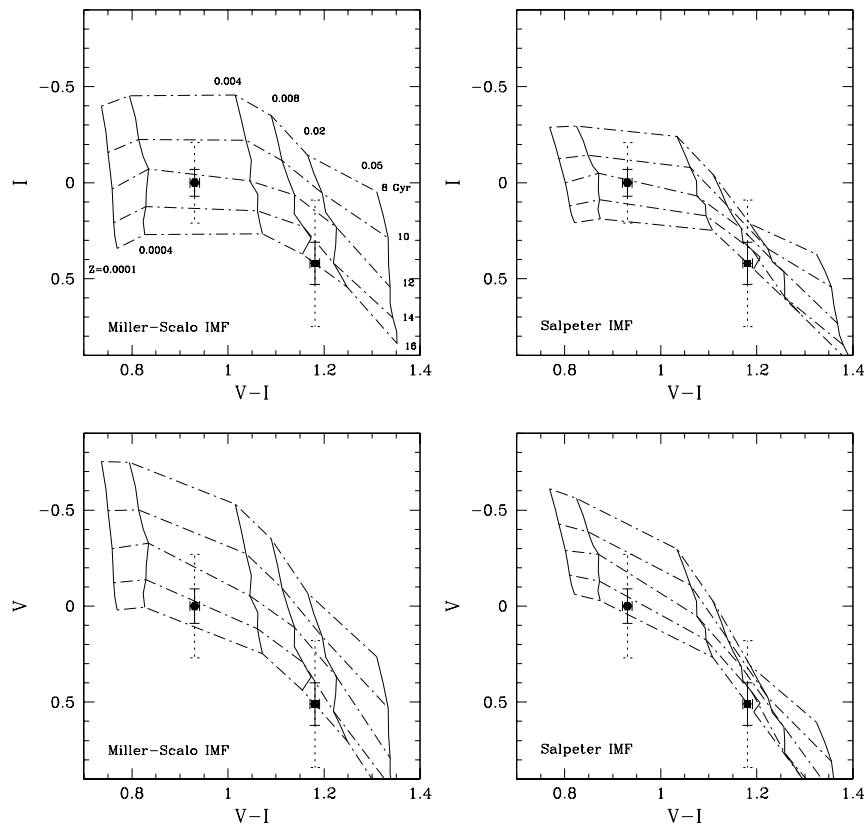
FIG. 10.—Simple stellar population models by Kurth et al. (1999) calculated for a single stellar burst of 10^7 Gyr duration. *Top panels*: I-band TO magnitudes. *Bottom panels*: V-band TO magnitudes. Within the grids the solid lines (*vertical*) represent isometallicity tracks of $Z = 0.0001, 0.0004, 0.004, 0.008, 0.02, 0.05$ (*left to right*) which correspond to [Fe/H] $= -2.3, -1.7, -0.7, -0.4, 0.0$, and 0.4. The dash-dotted (*horizontal*) lines are isochrones of 8, 10, 12, 14, and 16 Gyr. The solid error bars represent the 1 σ errors. The dotted error bars give the 3 σ deviations. An averaged maximum age difference of $\Delta T = -2.3 \pm 1.6$ Gyr is derived.

The age difference varies between -3.8 Gyr (Salpeter IMF, I band) and -0.4 Gyr (Salpeter IMF, V band) with a typical error of 2.2 Gyr. The mean difference is -2.3 ± 1.6 Gyr, i.e., the red population appears somewhat older than the blue one. The 3 σ differences are around -7 and $+2.5$ Gyr.

4.1.5. Comparison with Bruzual & Charlot (1996)

In Figure 11, we compare our results with the models of Bruzual & Charlot (1996). We used the single burst populations computed with a Salpeter (1955) IMF and a Scalo (1986) IMF, with metallicities between $Z = 0.0004$ and 0.05. Their models with a Miller & Scalo (1979) IMF were not used. The tracks for their highest metallicity ($Z = 0.1$) are not shown. The oldest modeled population is 16 Gyr.

The age differences vary between $+1$ Gyr (Scalo IMF, I band) and $+6$ Gyr (Salpeter IMF, V band), with an typical error of 2.8 Gyr. The mean difference is $+3.3 \pm 2.2$ Gyr. The 3σ limits lie around -3 and $+10$ Gyr.

4.1.6. Comparison with Worthey (1994)

In Figure 12, we compare our results with Worthey's (1994) single-burst models. He computed models with a Salpeter (1955) IMF and a Miller & Scalo (1985) IMF for metallicities between $Z = 0.0002$ and 0.05, up to an age of 16 Gyr.

The age difference varies between -5.8 Gyr (Salpeter IMF, I band) and -2.1 Gyr (Miller-Scalo IMF, V band), with a typical error of 2.5 Gyr. The mean difference is

-4.0 ± 1.6 Gyr, i.e., the red populations appears older than the blue one. The 3 σ limits are around -9 and $+1$ Gyr.

4.1.7. Maximum Age Difference between the Globular Cluster Populations

We note that the I band results give a systematically smaller difference (in the sense we defined it: age$_{blue}$ $-$ age$_{red}$) than the V band results. Except for the Bruzual & Charlot (1996) models, the results from the I band suggest that the red population is marginally older than the blue one.

The different models predict mean differences anywhere between -4.0 Gyr and $+3.3$ Gyr, with a mean of -0.6 Gyr and a dispersion of 3.2 Gyr. It would be somewhat arbitrary to assign more weight to one model than to another, so that we are currently limited in the age determination by the model uncertainties. Nevertheless, it seems that both populations are coeval within the errors, and we can exclude at the 99% confidence level one population being half as old as the other.

If our results are affected by a systematic error, e.g., if the smaller sizes of the red globular clusters do indeed translate into a lower "mean" mass (such that the red TO magnitude is $\simeq 0.2$ lower—see § 4.1.1), the age difference would be affected by $\simeq +4$ Gyr.

4.2. Implications for the Star Formation Episodes of NGC 4472

The above results suggest that the vast majority of globular clusters and stars formed at high redshift in this cluster
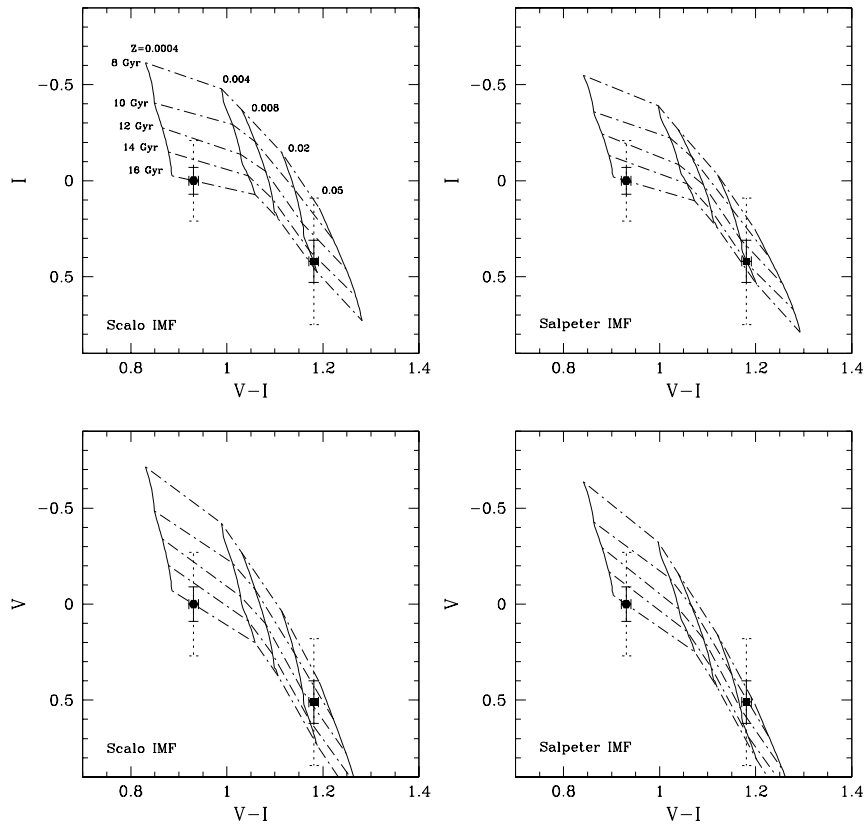
FIG. 11.—Simple stellar population models by Bruzual & Charlot (1996). *Top panels*: *I*-band data. *Bottom panels*: *V*-band data. The solid grid lines represent isometallicity tracks of $Z = 0.0004, 0.004, 0.008, 0.02$, and 0.05. Dash-dotted lines are isochrones of 8, 10, 12, 14, and 16 Gyr. Using these grids an averaged maximum-age difference of $\Delta T = 3.3 \pm 2.2$ Gyr was derived.
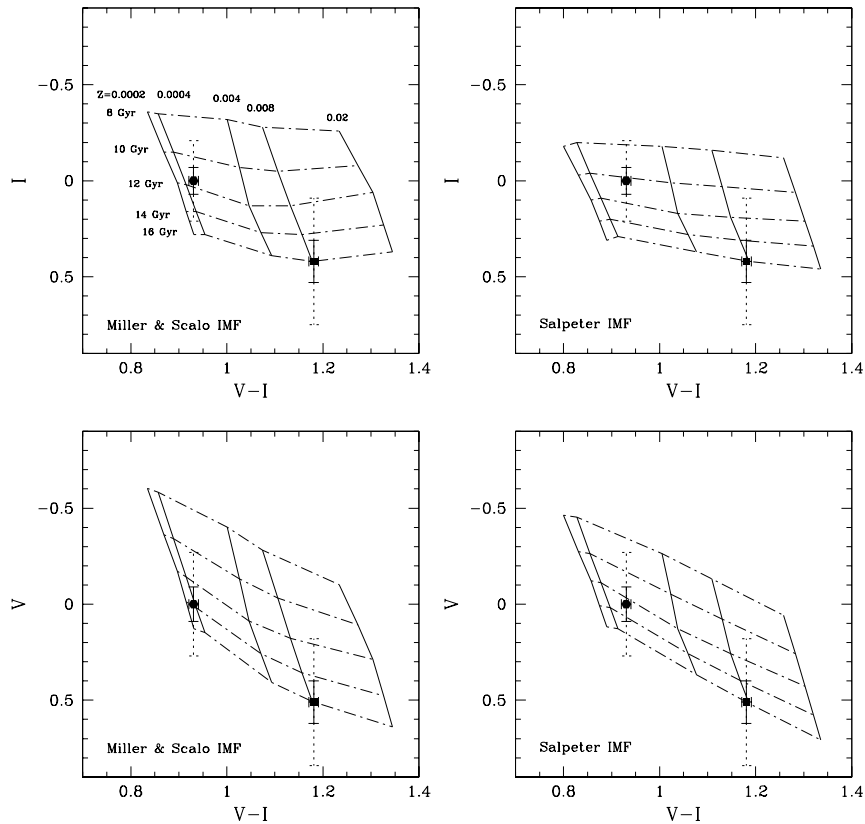

FIG. 12.—Worthey's (1994) simple stellar population models. *Top panels*: *I*-band data. *Bottom panels*: *V*-band data. The solid grid lines represent isometallicity tracks of $Z = 0.0002, 0.0004, 0.004, 0.008$, and 0.02. Dash-dotted lines are isochrones of 8, 10, 12, 14, and 16 Gyr. The averaged maximum age difference is $\Delta T = -4.0 \pm 1.6$ Gyr.

galaxy. As already mentioned in § 1, several other lines of evidence lead to similar results for cluster galaxies. Interestingly, the globular cluster results imply that two major star formation events took place at high redshift. Those two events appear to have happened moderately closely in time but from differently enriched gas. The blue clusters appear to have formed from gas with less than 1/20th solar metallicity, while the red clusters formed out of gas with close to solar metallicity. Furthermore, the mean sizes of the blue and red clusters appear to be significantly different. This suggests different conditions at the formation epoch, unless they are directly related to the metallicity and associated cooling processes in the molecular clouds in which the clusters originated.

It is unclear whether the blue or the red clusters are the older ones. At face value it seems odd that the more metal-rich clusters would be the older ones. However, in scenarios where the blue clusters formed in halo clouds (e.g., Kissler-Patig et al. 1998b) or were accreted with dwarf galaxies (e.g., Côté, Marzke, & West 1998; Hilker et al. 1999a, 1999b), this could be understood in terms of the large structures (e.g., bulges) collapsing first, followed shortly thereafter by the smaller structures (clouds/dwarf galaxies). This, however, would force a revision of the merger scenario, which clearly predicts that the red clusters will be younger than the blue ones.

Alternatively, if two subpopulations of clusters are coeval or if the blue clusters are the older ones, age differences of a few Gyr between the different subpopulations could be explained in all globular cluster/galaxy formation scenarios, i.e., the above-mentioned scenarios, merging (Ashman & Zepf 1992), or in situ formation of distinct populations (e.g., Forbes, Brodie, & Grillmair 1997; Harris et al. 1998; Harris, Harris, & Poole 1999). We note only that, in the merger scenario, merging would have to have taken place at early times ($z > 1$ at the 3 σ level), which is somewhat at odds with the recent theoretical predictions from hierarchical clustering models (e.g., Kauffmann 1996; Baugh et al. 1998). These tend to predict that the main star formation in cluster environments occurred at redshifts $z < 1$.

5. A DISTANCE ESTIMATION FOR NGC 4472

The TO magnitude (V_{TO}) of the GCLF appears to be essentially universal and, therefore, can be used as a distance indicator (e.g., the review by Whitmore 1997). V_{TO} depends on the age and metallicity of the globular clusters (Ashman et al. 1995, see also § 4.1) and weakly on galaxy type (Harris 1997), which may be a consequence of the age/metallicity dependence. The derived TO magnitude for the globular clusters in NGC 4472 can be used to obtain a distance to the galaxy.

5.1. Absolute Turnover Magnitude

The method is best calibrated using the TO magnitude of the Milky Way GCLF, since it involves the minimum number of steps on the distance ladder. The M31 GCLF serves as a strong check on this calibration (see Ferrarese et al. 2000; Kavelaars et al. 1999).

The Milky Way system is dominated by old globular clusters of mean metallicity [Fe/H] $\simeq -1.4$. It is, therefore, well suited to fitting the TO magnitude of the blue population in NGC 4472 (see § 4.1) and no correction for age-metallicity dependence need be applied. However, we have to assume that age-metallicity dominates any dependence

on galaxy type and that globular cluster mass functions are intrinsically similar, which seems justified to first order (e.g., Kissler-Patig et al. 1998b).

Della Valle et al. (1998) recently rederived V_{TO} for the Milky Way system. To derive individual distances to all Galactic globular clusters, they adopted a horizontal branch (HB) magnitude-metallicity relation derived from globular cluster main sequence fitting using distance measurements to subdwarfs from *Hipparcos* (in this case by Gratton et al. 1997). From the resulting GCLF they obtained $V_{TO} = -7.62 \pm 0.06$, noting that, depending on the adopted HB magnitude-metallicity relation, this result could suffer from a 0 to -0.2 mag systematic error.

Drenkhahn & Richtler (1999) used a different approach. They assumed the LMC distance to be the fundamental zero point (here $(m - M) = 18.46 \pm 0.06$), and derived an RR Lyrae magnitude-metallicity relation. The remaining steps were similar to those of Della Valle et al. Drenkhahn & Richtler found $V_{TO} = -7.61 \pm 0.08$ and $I_{TO} = -8.48 \pm 0.10$ for the Milky Way GCLF.

5.2. Distance to NGC 4472

The apparent TO magnitude derived for the blue population is $V_{TO} = 23.62 \pm 0.09$ and $I_{TO} = 22.48 \pm 0.07$ (see Table 3). These values need to be corrected for the photometric term discussed in § 2.2.3 ($\Delta C_V = 0.050 \pm 0.015$, $\Delta C_I = 0.080 \pm 0.010$), as well as for Galactic extinction ($A_V = 0.069$, $A_I = 0.040$). Using the absolute TO magnitudes discussed above, we derive distance moduli of $(m - M)_V = 31.11 \pm 0.19$ and $(m - M)_I = 30.84 \pm 0.14$ (adding all errors in quadrature), i.e., a mean $(m - M) = 30.99 \pm 0.11$ (where the error does not include any possible systematic error in the calibration). The corresponding distance is 15.8 ± 0.8 Mpc.

A quick comparison with distances derived for NGC 4472 by other methods shows very good agreement (despite completely different calibrations). Jacoby, Ciardullo, & Ford 1990) derived $(m - M) = 30.84 \pm 0.11$ from the planetary nebulae luminosity function. Tonry, Ajhar, & Luppino (1990) and Neilsen (1999) derived $(m - M) = 30.78 \pm 0.07$ and $(m - M) = 30.93 \pm 0.08$, respectively, from surface brightness fluctuations.

Cepheid distances now exist for seven spiral galaxies in the Virgo Cluster (see Pierce et al. 1994 and Ferrarese et al. 2000). With the exception of NGC 4639 (Saha et al. 1996), which appears to be background to the main body of spirals, the mean distance to the other six galaxies is $(m - M) = 31.01 \pm 0.07$ or 16.0 ± 0.6 Mpc. Our GCLF distance to NGC 4472 is in excellent agreement with this distance, which supports the view that the Virgo Cluster spirals and ellipticals are at essentially the same distance.

6. SUMMARY

The age difference between the two major globular cluster subpopulations in an early-type galaxy has been determined. We have developed an age differentiating method that uses the precise TO magnitudes and colors of the subpopulations. We have applied this method to NGC 4472, matching our observables to several SSP synthesis models.

An extended-object analysis showed that at the distance of Virgo (i.e., ~16 Mpc) *HST* is capable of resolving single globular clusters. Thus it is necessary to make an additive

correction (of $C_V = 0.050 \pm 0.015$ mag and $C_I = 0.080 \pm 0.010$ mag at the distance of Virgo) to the mean correction of $C = 0.1$ mag (for point sources) when extrapolating *HST* photometry obtained in 0″5 radius apertures to total luminosities. This corresponds to a color correction of $C_{(V-I)} = 0.03 \pm 0.018$.

We found the globular cluster color distribution in NGC 4472 to be clearly bimodal (at the 99.99% confidence level) with two peaks located at $V-I = 0.99 \pm 0.01$ and 1.24 ± 0.01 corresponding to $(V-I)_0 = 0.93 \pm 0.02$ and $(V-I)_0 = 1.18 \pm 0.02$ when corrected for reddening and finite aperture. We determined that the red globular clusters have a color distribution almost twice as broad as the blue ones.

We divided the whole globular cluster population into an inner and an outer sample, as defined by the *HST* different pointings. We used an improved maximum-likelihood estimator, which accounts for varying background values, to determine the TO magnitudes for each subpopulation in each radial sample (see Table 3). The TO of the blue subpopulation is the same for the inner and outer sample. By contrast, the red subpopulation appears to be marginally brighter by 0.27 ± 0.14 mag in the inner region than in the outer region. This difference is of the expected order of magnitude if destruction processes act on the red sample within 5 kpc.

The radial color distributions of each subpopulation show almost no gradients. However, we detected an overall gradient of $\Delta(V-I)/\Delta \log r = -0.029 \pm 0.07$ mag $[\log (\mathrm{arcsec})]^{-1}$ in the system, which is mostly an effect of the changing ratio of red to blue globular clusters with radius (see Geisler et al. 1996).

Taking advantage of *HST*'s high spatial resolution, we estimated the mean sizes of the globular clusters using the $\Delta(0.5 - 3)$ parameter. The blue globular clusters were found to be larger than the red ones, as was already observed in M87 (Kundu et al. 1999) and NGC 3115 (Kundu & Whitmore 1998). The most likely explanations are that the size

difference reflects different formation processes or that red clusters are on preferentially radial orbits, while blue clusters are on preferentially tangential orbits.

We used four different SSP models to derive the mean age difference between the red and blue subpopulation. Our underlying assumption was that both blue and red populations have similar mass distributions, which appears to be valid at least at the 10% to 20% level (which, nevertheless, corresponds to a potential systematic error of ~ 4 Gyr). The mean age difference between the blue (metal-poor) and the red (metal-rich) subpopulations is $\mathrm{age_{blue}} - \mathrm{age_{red}} = -0.6 \pm 3.2$ Gyr, where the error is the dispersion introduced by the different models (for a given model the error on our method is ~ 2 Gyr).

We conclude that the globular clusters (and by association the stars) in NGC 4472 formed in two major episodes/mechanisms that were coeval within a few Gyr.

The images as well as electronic lists of the photometry are available from the authors. Also available is the maximum-likelihood code as an IRAF task used to derive the globular cluster luminosity functions taking into account the background variations over the field.

REFERENCES

Ajhar, E. A., Blakeslee, J. P., & Tonry, J. L. 1994, AJ, 108, 2087
Ashman, K. M., Bird, C. M., & Zepf, S. E. 1994, AJ, 108, 2348
Ashman, K. M., Conti, A., & Zepf, S. E. 1995, AJ, 110, 1164
Ashman, K. M., & Zepf, S. E. 1992, ApJ, 384, 50
———. 1998, Globular Cluster Systems (Cambridge: Cambridge Univ. Press)
Baugh, C. M., Cole, S., Frenk, C. S., & Lacey, C. G. 1998, ApJ, 498, 504
Bender, R. 1997, in ASP Conf. Ser. 116, The Nature of Elliptical Galaxies, ed. M. Arnaboldi, G. S. Da Costa, & P. Saha (San Francisco: ASP), 11
Bertin, E., & Arnouts, S. 1996, A&AS, 117, 393
Bevington, P. R., & Robinson, D. K. 1992, Data Reduction and Error Analysis for the Physical Sciences (2d ed.; New York: McGraw-Hill)
Brodie, J. P., Schroder, L. L., Huchra, J. P., Phillips, A. C., Kissler-Patig, M., & Forbes, D. A. 1998, AJ, 116, 691
Bruzual, A. G., & Charlot, S. 1996, electronically available see: Leitherer, C., et al. 1996, PASP, 108, 996
Burstein, D., & Heiles, C. 1982, AJ, 87, 1165
Cohen, J. G. 1988, AJ, 95, 682
Cohen, J. G., Blakeslee, J. P., & Ryzhov, A. 1998, ApJ, 496, 808
Côté, P., Marzke, R. O., & West, M. 1998, ApJ, 501, 554
Couture, J., Harris, W. E., & Allwright, J. W. B. 1990, ApJS, 73, 671
———. 1991, ApJ, 372, 97
Dean, J. F., Warren, P. R., & Cousins, A. W. J. 1978, MNRAS, 183, 569
Della Valle, M., Kissler-Patig, M., Danziger, J., & Storm, J. 1998, MNRAS, 299, 267
de Vaucouleurs G., de Vaucouleurs, A., Corwin, H. G., Jr., Buta, R. J., Paturel, G., & Fouqué, P. 1991, Third Reference Catalogue of Bright Galaxies (version 3.9; New York: Springer)
Drenkhahn, G. 1999, thesis, Univ. Bonn
Drenkhahn, G., & Richtler, T. 1999, A&A, in press

Dubath, P., & Grillmair, C. J. 1997, A&A, 321, 379
Elmegreen, B. G., & Efremov, Y. N. 1997, ApJ, 480, 235
Ferrarese, L., et al. 2000, ApJ, in press
Forbes, D. A., Brodie, J. P., & Grillmair, C. J. 1997, AJ, 113, 1652
Gebhardt, K., & Kissler-Patig, M. 1999, AJ, 118, 1526
Geisler, D., Lee, M. G., & Kim, E. 1996, AJ, 111, 1529
Gnedin, O. Y., & Ostriker, J. P. 1997, ApJ, 474, 223
Gould, A., Flynn, C., & Bahcall, J. N. 1998, ApJ, 503, 798
Gratton, R. G., Fusi Pecci, F., Carretta, E., Clementini, G., Corsi, C. E., & Lattanzi, M. 1997, ApJ, 491, 749
Harris, G. H. L., Harris, W. E., & Poole, G. B. 1999, AJ, 117, 855
Harris, W. E. 1996, AJ, 112, 1487
———. 1997, The Extragalactic Distance Scale, ed. M. Livio, M. Donahue, & N. Panagia (Cambridge: Cambridge Univ. Press), 29 (poster)
Harris, W. E., Allwright, J. W. B., Pritchet, C. J., & van den Bergh, S. 1991, ApJS, 76, 115
Harris, W. E., Harris, G. L. H., & McLaughlin, D. E. 1998, AJ, 115, 1801
Harris, W. E., & van den Bergh, S. 1981, AJ, 86, 1627
Hilker, M., Infante, L., Vieira, G., Kissler-Patig, M., & Richtler, T. 1999a, A&AS, 134, 75
Hilker, M., Kissler-Patig, M., Richtler, T., Infante, L., & Quintana, H. 1999b, A&AS, 134, 59
Holtzman J., et al. 1995, PASP, 107, 1065
Jacoby, G. H., Ciardullo, R., & Ford, H. C. 1990, ApJ, 356, 332
Kauffmann, G. 1996, MNRAS, 281, 487
Kavelaars, J. J., Harris, W. E., Hanes, D. A., Hesser, J. E., & Pritchet, C. J. 1999, ApJ, in press
Kissler-Patig, M., et al. 1998a, AJ, 115, 105
Kissler-Patig, M., Forbes, D. A., & Minniti, D. 1998b, MNRAS, 298, 1123
Kissler-Patig, M., & Gebhardt, K. 1998, AJ, 116, 2237
Kissler-Patig, M., Richtler, T., Storm, J., & Della Valle, M. 1997, A&A, 327, 503

Krist, J., & Hook, R. 1997, TinyTim User's Handbook (version 4.4; Baltimore: STScI)
Kundu, A., & Whitmore, B. C. 1998, AJ, 116, 2841
Kundu, A., Whitmore, B. C., Sparks, W. B., Macchetto, F. D., Zepf, S. E., & Ashman, K. M. 1999, ApJ, 513, 733
Kurth, O. M., Fritze-v. Alvensleben, U., & Fricke, K. J. 1999, A&AS, 138, 19
Larsen, S. S., & Richtler, T. 1999, A&A, 345, 59
Laurent-Muehleisen, S. A., Kollgaard, R. I., Ryan, P. J., Feigelson, E. D., Brinkmann, W., & Siebert, J. 1997, A&AS, 122, 235
Lee, M. G., & Geisler, D. 1993, AJ, 106, 493
Lee, M. G., Kim, E., & Geisler, D. 1998, AJ, 115, 947
Maraston, C. 1998, MNRAS, 300, 872
McLaughlin, D. E. 1999, AJ, in press
McLaughlin, D. E., & Pudritz, R. E. 1996, ApJ, 457, 578
Miller, G. E., & Scalo, J. M. 1979, ApJS, 41, 513
Neilsen, E. H., Jr. 1999, Ph.D. thesis, Johns Hopkins Univ.
Ortolani, S., et al. 1995, Nature, 377, 701
Pierce, M., et al. 1994, Nature, 371, 385
Poulain, P. 1988, A&AS, 72, 215
Renzini, A. 1999, in When and How Do Bulges Form? ed. C. M. Carollo, H. C. Ferguson, & R. F. G Wyse (Cambridge: Cambridge Univ. Press), in press
Rosenberg, A., Saviane, I., Piotto, G., & Aparicio, A. 1999, AJ, 118, 2306
Saha, A., et al. 1996, ApJ, 466, 55

Salpeter, E. E. 1955, ApJ, 121, 161
Scalo, J. M. 1986, The Stellar Initial Mass Function (New York: Gordon and Breach Sci.)
Schlegel, D. J., Finkbeiner, D. P., & Davis, M. 1998, ApJ, 500, 525
Schweizer, F. 1997, in ASP Conf. Ser. 116, The Nature of Elliptical Galaxies, ed. M. Arnaboldi, G. S. Da Costa, & P. Saha (San Francisco: ASP), 447
Schweizer, F., Miller, B. W., Whitmore, B. C., & Fall, S. M. 1996, AJ, 112, 1839
Secker, J. 1992, AJ, 104, 1472
Sharples, R. M., Zepf, S. E., Bridges, T. J., Hanes, D. A., Carter, D., Ashman, K. M., & Geisler, D. 1998, AJ, 115, 2337
Silverman, B. W. 1986, Density Estimation for Statistics and Data Analysis, Monographs on Statistics and Applied Probability, Vol. 26 (London: Chapman & Hall)
Tonry, J. L., Ajhar, E. A., & Luppino, G. A. 1990, AJ, 100, 1416
van den Bergh, S. 1994, AJ, 108, 2145
Vesperini, E. 1998, MNRAS, 289, 1019
Whitmore, B. C. 1997, The Extragalactic Distance Scale, ed. M. Livio, M. Donahue, & N. Panagia (Cambridge: Cambridge Univ. Press), 254
Williams, R. E., et al. 1996, AJ, 112, 1335
Worthey, G. 1994, ApJS, 95, 107
Zepf, S. E., & Ashman, K. M. 1993, MNRAS, 264, 611

ERRATUM: "THE AGE DIFFERENCE BETWEEN THE GLOBULAR CLUSTER SUBPOPULATIONS IN NGC 4472" [ASTRON. J. **118**, 2734 (1999)]

THOMAS H. PUZIA
Sternwarte der Universität Bonn and UCO/Lick Observatory

MARKUS KISSLER-PATIG
European Southern Observatory and UCO/Lick Observatory

JEAN P. BRODIE
UCO/Lick Observatory

AND

JOHN P. HUCHRA
Harvard-Smithsonian Center for Astrophysics
Received 2000 May 4; accepted 2000 May 4

We report on a systematic error introduced in our photometry of globular clusters around NGC 4472. The photometry included an aperture correction of 0.1 mag (following J. Holtzman, C. J. Burrows, S. Casertano, J. J. Hester, J. T. Trauger, A. M. Watson, & G. Worthey, PASP, 107, 1065 [1995]), as stated in the footnote of our Table 3, only appropriate for surface brightness photometry of extended sources. The extended nature of the clusters, however, was already taken into account by our correction terms C_V and C_I. Thus, all V and I magnitudes should be recorrected by $+0.1$ mag. *The colors remain unchanged, as do magnitude differences.* For general uncertainties of WFPC2 calibrations, see P. Stetson (PASP, 110, 1448 [1998]) and B. Whitmore, I. Heyer, & S. Casertano (PASP, 111, 1559 [1999]).

This systematic error has absolutely no impact on our conclusions, since these were only based on colors and relative magnitudes (the *difference* between the globular cluster luminosity function turnover for the blue and red globular clusters). However, all values M_{TO} in our Table 3 need to be corrected by $+0.1$ mag. Our corrected weighted mean distance modulus to NGC 4472 is $m - M = 31.04 \pm 0.11$, corresponding to a distance of $16.1^{+0.9}_{-0.8}$ Mpc. This is still in very good agreement with the mean distance derived from six Virgo galaxies with Cepheid measurements: $m - M = 31.01 \pm 0.07$, or 16.0 ± 0.6 Mpc.

We are grateful to M. G. Lee for pointing out the calibration bias.